Review

Converging on the function of intrinsically disordered nucleoporins in the nuclear pore complex

Orit Peleg[1] and Roderick Y.H. Lim[2,*]

[1] Polymer Physics, Department of Materials, ETH Zurich, Wolfgang-Pauli-Strasse 10, CH-8093 Zurich, Switzerland
[2] Biozentrum and the Swiss Nanoscience Institute, University of Basel, Klingelbergstrasse 70, CH-4056 Basel, Switzerland

*Corresponding author
 e-mail: roderick.lim@unibas.ch

Abstract

Several biological mechanisms involve proteins or protein-aceous components that are intrinsically disordered. A case in point pertains to the nuclear pore complex (NPC), which regulates molecular transport between the nucleus and the cytoplasm. NPC functionality is dependent on unfolded domains rich in Phe-Gly (FG) repeats (i.e., FG-domains) that collectively act to promote or hinder cargo translocation. To a large extent, our understanding of FG-domain behavior is limited to *in vitro* investigations given the difficulty to resolve them directly in the NPC. Nevertheless, recent findings indicate a collective convergence towards rationalizing FG-domain function. This review aims to glean further insight into this fascinating problem by taking an objective look at the boundary conditions and contextual details under-pinning FG-domain behavior in the NPC. Here, we treat the FG-domains as being commensurate with polymeric chains to address ambiguities such as for instance, how FG-domains tethered to the central channel of the NPC would behave differently as compared with their free-floating counterparts in solution. By bringing such fundamental questions to the fore, this review seeks to illuminate the importance of how such parameters can hold influence over the structure-function relation of intrinsically disordered proteins in the NPC and beyond.

Keywords: FG-domains; hydrogel; intrinsically unstructured proteins; nanopore; natively unfolded proteins; nucleocytoplasmic transport; polymer brush.

Introduction

The compartmentalization of the eukaryotic cell necessitates that biochemically specific molecules are targeted to the correct spatial location for cellular processes to proceed. In this regard, proteins and mRNA (generally termed cargo) are continuously being exchanged across the nuclear envelope (NE) separating the nucleus and the cytoplasm. This is known as nucleocytoplasmic transport (NCT), and occurs through numerous pore-like perforations in the NE, called nuclear pore complexes (NPCs) (Lusk et al., 2007; Stewart, 2007; D'angelo and Hetzer, 2008; Lim et al., 2008; Terry and Wente, 2009).

As the only passageway in and out of the nucleus, the intrigue behind the NPC lies in its ability to sieve out and select specific molecules destined for NCT. Each NPC is a large macromolecular complex composed of approximately 30 distinct proteins, known as nucleoporins (Nups) (Rout et al., 2000; Cronshaw et al., 2002). Based on the eight-fold symmetry of the NPC (Yang et al., 1998; Stoffler et al., 2003; Beck et al., 2004; Alber et al., 2007a,b; Beck et al., 2007; Frenkiel-Krispin et al., 2010), each Nup is thought to be present in multiples of eight, amounting to an overall mass of approximately 60 MDa (Rout and Blobel, 1993) and approximately 120 MDa (Reichelt et al., 1990) for the yeast and vertebrate NPC, respectively. The Nups can be categorized into two structural sub-groups. One category consists of structured Nups that anchor the NPC to the NE and act as the building blocks that give the NPC its overall structure and shape (Devos et al., 2006). Another category of Nups is located in and around the central channel of the NPC and consists of large natively unfolded domains that are rich in phenylalanine-glycine (FG)-repeat motifs (i.e., FG-domains; Denning et al., 2003). Altogether, these components give the NPC a characteristic size of between 50 and 100 nm depending on the species (Yang et al., 1998; Stoffler et al., 2003; Beck et al., 2004, 2007; Alber et al., 2007a,b; Elad et al., 2009; Frenkiel-Krispin et al., 2010) (Figure 1).

When considered in physical terms, the biological marvel of the NPC lies in its ability to restrict or promote cargo translocation via biochemical selectivity and not size exclusion *per se*. In comparison to small molecules (e.g., water and ions) that diffuse freely through its central channel, macromolecular translocation across the NPC is largely regulated for cargoes greater than 40 kDa in mass (Keminer and Peters, 1999). Broadly speaking, specific cargoes are identified by transport receptors (i.e., karyopherins or Kaps but more specifically, importins and exportins) through a sequence of residues known as nuclear localization/export signals (i.e., NLS/NES) (Rexach and Blobel, 1995; Gorlich and Kutay, 1999; Pemberton and Paschal, 2005; Stewart, 2007). By binding with the Kaps, the cargo is then targeted to the NPC for exclusive translocation. In the absence of Kaps, macromolecular access through the NPC is inhibited. NCT directionality is driven by the GTPase Ran, which functions as a molecular ratchet between its GTP- and GDP-bound forms
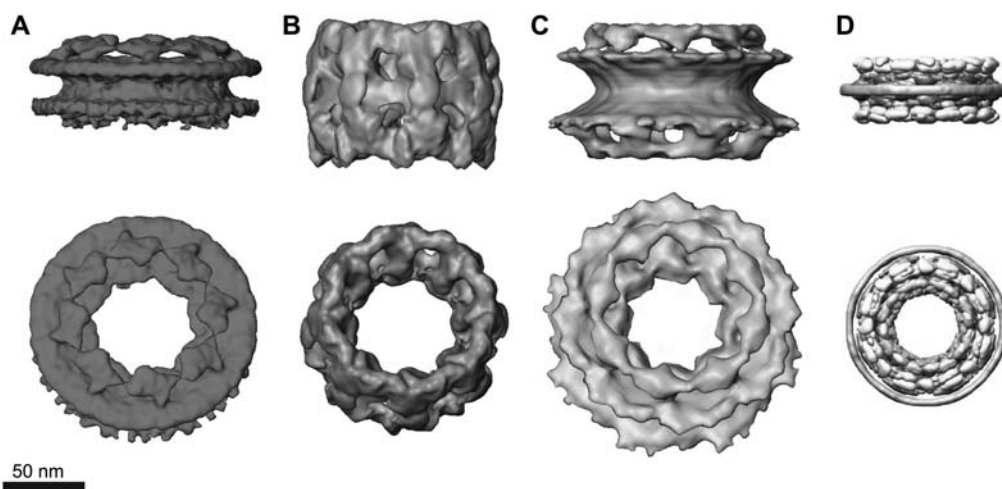
Figure 1   Three-dimensional reconstructions of NPCs.

(A) *Dictyostelium discoideum*, (B) *Xenopus* oocytes, (C) *Homo sapiens* as derived by cryo-electron tomography. (D) *Saccharomyces cerevisiae* by *in silico* reconstruction. Luminal and cytoplasmic faces of the NPCs are shown in the upper and lower panels, respectively. The height of the central framework varies between species. Information regarding the FG-domains and/or their anchoring sites is lacking. (A), (B) and (C) were taken from Elad et al. (2009). (D) Has been modified with permission from Alber et al. (2007b).

localized to the nucleus and cytoplasm, respectively (Gorlich et al., 1996). In the case of nuclear import, RanGTP binding triggers cargo release whereas export is dependent on the hydrolysis of RanGTP to RanGDP for cargo release into the cytoplasm (Conti et al., 2006).

The NPC paradox

Not least for its potential technological appeal (Jovanovic-Talisman et al., 2009), the dualistic functionality of the NPC to act as a permeability barrier that impedes the passage of passive macromolecules while facilitating the translocation of Kap-cargo complexes has remained the center of immense interest. Paradoxically, a large cargo can only gain exclusive access through the NPC in complex with a Kap, which in many cases more than doubles its overall mass. Therefore, cargo translocation is not governed by size exclusion *per se*.

Several lines of evidence indicate that the unfolded FG-domains form the primary physical constituents of this gating mechanism. Each NPC consists of approximately 12 different FG-Nups amounting to approximately 200 FG-domains per NPC (Rout et al., 2000; Cronshaw et al., 2002). The FG-domains can be further classified by their FG-repeat motifs, such as GLFG, FxFG and FG, although several FG-domains comprise more than one type of repeat (summarized in Table 1). Cargo selection relies on biochemical binding interactions between Kaps and the FG-repeat motifs (Radu et al., 1995; Bayliss et al., 1999, 2000, 2002a,b; Cushman et al., 2006). In doing so, Kap-FG binding is thought to somehow cause a transient breach or opening in the NPC barrier to make space for translocation to proceed. What is perhaps more intriguing is how the NPC does not seem to clog under physiological conditions, in spite of the molecular complexity and crowding (Zimmerman and Minton, 1993) within the cellular environment. This is in marked contrast to synthetic nanopores (Belfort et al., 1994), which suffer from the aggregation of non-specific material (also known as fouling; Hong and Elimelech, 1997; Koehler et al., 1997) in and around their pores and hence are often prone to 'getting stuck'.

NPC models

The exact manner by which the FG-domains contribute to the NPC gating mechanism is still being actively debated. Nevertheless, it is generally accepted that the collective behavior of the FG-domains acts as a barrier to non-specific cargo translocation in and around the NPC (Lim et al., 2008). In spite of their variety, these models differ only in the physical arrangement and mobility (static vs. dynamic) of the FG-domains within the NPC. So far, studies targeting the materials properties of the FG-domains directly show that FG-domain behavior can be classified as resembling (i) a polymer brush (Lim et al., 2006, 2007a; Miao and Schulten, 2009) (i.e., dynamic), (ii) a bulk-like hydrogel meshwork (Frey et al., 2006; Frey and Gorlich, 2007, 2009) (i.e., static) or (iii) both (Patel et al., 2007). Here, we outline the differences between these characteristics and will attempt to address their convergent properties later on.

Brush-like models

Being tethered on one end to the inner surface of the central channel, brush-like models postulate that the FG-domains can somehow form a barrier at the NPC by extending out into the solution. Originally, the 'Brownian affinity gating' model (Rout et al., 2000) (also known as 'virtual gating'; Rout et al., 2003) postulated that the mobile FG-domains can

Table 1 Properties of *S. cerevisiae* and *H. sapiens* FG-domains.

	FG-domain[a]	Number of amino acids	Cohesive[b] (Y/N)	% Positive[c]	% Negative[c]	% Net charge	% Hydrophobic[d]	Number of repeat motifs			
								FxFG[e]	GLFG[e]	FG[e]	FxF[e]
S. cerevisiae											
Nup42	1–374	373	Y	3.21	0.53	2.67	24.87	2	0	28	0
Nup49	1–417	416	Y	5.76	6.00	-0.24	27.34	2	8	9	0
Nup57	1–365	364	Y	4.66	2.74	1.92	22.47	2	9	9	0
Nup100	1–884	883	Y	5.2	3.96	1.24	22.96	0	11	35	0
Nup145	1–367	366	Y	5.18	3.27	1.91	25.07	3	7	3	0
Nup116	1–696	695	Y	2.59	1.01	1.58	23.28	0	20	27	1
Nsp1	3–601	598	N	11.85	10.35	1.5	23.87	20	0	14	1
Nup60	387–521	134	N	11.85	14.07	-2.22	25.19	1	0	0	3
Nup159	454–855	401	N	7.21	11.44	-4.23	24.38	2	0	23	0
Nup1	325–1049	724	N	9.38	8.14	1.24	24.69	15	0	4	8
Nup2	206–562	356	N	12.32	12.04	0.28	23.81	11	0	0	3
Nup53	41–267	226	–	9.25	11.01	-1.76	28.63	0	0	4	0
Nup59	1–206	205	–	7.77	5.83	1.94	20.39	0	0	4	0
H. sapiens											
Nup54	1–340	339	–	7.06	7.06	0.00	32.06	1	1	10	1
Nup62	1–300	299	–	1.33	0.00	1.33	32.33	12	0	5	0
Nup45	1–463	462	–	6.91	5.83	1.08	32.61	4	1	8	0
Nup214	1664–2090	426	–	1.87	0.7	1.17	29.27	4	1	42	1
Nup58	1–499	498	–	6.81	6.41	0.4	32.26	3	1	8	0
Nup98	1–646	645	–	5.88	3.72	2.17	25.85	2	9	34	1
Cg1/Nlp1	4–375	371	–	8.6	6.72	1.88	29.57	0	0	16	2
Pom121	587–963	376	–	1.59	0.8	0.8	35.54	5	0	17	1
Nup153	477–1448	971	–	7.3	7.1	0.21	27.16	19	0	20	5
Nup50	39–236	197	–	11.11	7.58	3.54	30.81	0	0	5	0
Nup358	1511–2271	760	–	12.48	12.61	-0.13	27.33	10	0	11	3

[a]The FG-domains are defined as the largest contiguous sequence of amino acids containing the FG motifs FxFG, GLFG, FG, FxF and their reverse sequences (using this order of priority in case of overlaps), separated by <100 amino acids and including 10 additional amino acids at the termini of the domain.

[b]Defined according to Patel et al. (2007).

[c]The percentage of charge at pH 7.2 is the relative amount of positively charged amino acids (Lys, Arg) and negatively charged amino acids (Asp, Glu).

[d]The percentage of hydrophobic amino acids is based on the relative amounts of Ala, Ile, Leu, Phe, Trp and Val.

[e]Reverse sequences included (i.e., GFxF, GFLG and GF).

give rise to an entropic barrier that sterically hinders non-specific cargoes from entering the NPC. Next, the 'oily spaghetti' model (Macara, 2001) described the FG-domains as being loose extended chains that lined the inner NPC walls, leaving a cylindrical, tube-like space of approximately 10 nm in diameter that remained unoccluded by the FG-domains at the very pore center. The FG-domains would then be easily 'pushed aside' by transient Kap-FG interactions for cargo translocation to proceed. Indeed, the mobility of FG-domains has been inferred from immunolabeling electron microscopy based on variations in their localization within the NPC (Fahrenkrog et al., 2002; Lim et al., 2007a). Later, *in vitro* evidence obtained using biophysical atomic force microscope (AFM) measurements showed that the FG-domain of Nup153 could act collectively as a polymer brush when end-tethered to 100 nm gold nanostructures (Lim et al., 2006, 2007a).

By definition, polymer brush formation occurs when end-tethered polymeric chains extend and stretch in a net perpendicular direction away from a surface under dense packing conditions in a good solvent. In this way, surfaces covered in polymer brushes frequently exhibit a property of resistance to non-specific adsorption and material accumulation owing to an exponential, long-range repulsive force that is generated by the brush (Degennes, 1987). With regard to the NPC, this suggests that brush-like FG-domains could collectively give rise to a corona-like or cloud-like steric barrier in and around the central channel that could repel non-specific cargoes and might explain why the NPC does not clog *in vivo*. In poor solvents, polymer brushes are known to collapse into tight compact structures owing to the dominance of intra-chain interactions over weak chain-solvent interactions (Minko, 2006). Interestingly, the FG-domain brush of Nup153 was shown to reversibly collapse by switching between 5% hexanediol (i.e., poor solvent) and PBS buffer, respectively (Lim et al., 2006). This supported the observation that hexanediol causes a non-selective opening of the NPC in transport assays (Ribbeck and Gorlich, 2002; Shulga and Goldfarb, 2003).

To explain how specific cargoes translocate through the FG-domain brush, it was observed within the NPC by immunolabeling electron microscopy and by *in vitro* biophysical AFM measurements that Kapβ1 (importinβ)-FG binding also causes a collapse of the FG-domains (Lim et al., 2007a). The FG-domain collapse could be subsequently reversed upon the introduction of RanGTP, which was explained to prevent further binding of the Kapβ1 molecules to the FG-domains. Although these observations were of a static (i.e., not time-dependent) nature, they indicate that Kap (un)binding can cause the FG-domains to undergo transient conformational changes, such as by collapsing and distending (i.e., akin to being 'pushed aside'; Macara, 2001) in a rapid, stochastic manner during cargo transport (Lim et al., 2007a). Nevertheless, it remains to be shown whether differences in Kap-FG binding affinities (Ben-Efraim and Gerace, 2001; Bednenko et al., 2003; Pyhtila and Rexach, 2003) between the various Kaps and FG-domains also result in similar collapse phenomena.

Gel-like models

Ribbeck and Görlich first proposed that the FG-domains could resemble a sieve-like meshwork or 'selective phase' within the NPC based on hydrophobic interactions between neighboring FG-repeats (Ribbeck and Gorlich, 2001). They subsequently showed and explained that mild apolar solvents (e.g., hexanediol) could cause a reversible collapse in the FG-domain barrier by perturbing the hydrophobic inter-FG interactions (Ribbeck and Gorlich, 2002). Subsequently through extensive investigations, Görlich and co-workers have since shown that FG-domains can form crosslinked macroscopic hydrogels from solution (Frey et al., 2006; Frey and Gorlich, 2007, 2009). Interestingly, Frey et al. showed hydrogel formation for both FG-/FxFG- (Nsp1) and GLFG-domains (Nup49 and Nup57) (Frey and Gorlich, 2009). They went on to show that these FG-domain hydrogels could reproduce the permeability properties of the NPC provided that the gels are saturated, i.e., every FG-repeat participates in a crosslink (Frey and Gorlich, 2007, 2009).

The selective phase model predicts that the spacing between each mesh (estimated to be between 3 and 6 nm based on the length of one repeat unit; Frey and Gorlich, 2007, 2009) defines the size limit for free diffusion through the hydrogel. Selective transport could then occur through catalytic binding of the Kap to individual FG-repeats that would effectively break individual cross-links without requiring any additional energy (Kustanovich and Rabin, 2004). In further support of the model, the retention of inert cargoes in solution during receptor-led transport indicates that the FG hydrogels possess a 'self-healing' property that could be important in the NPC (Frey and Gorlich, 2009). It is not clear, however, how hydrogel formation can take place in the NPC based on the differences between the *in vitro* requirements for gelation and *in vivo* conditions in the cell.

Other models

In vitro micro-bead binding assays used to classify the affinity of the different FG-domains showed that the FxFG-domains are non-cohesive as compared with the cohesive GLFG-domains (Patel et al., 2007). By correlating these properties to their estimated localizations in the NPC, the 'two-gate' model (Patel et al., 2007) proposes that the central channel is occupied by a FG-hydrogel whereas the FG-domains at the peripheries are brush-like. However, conflicting reports remain as to the observed non-cohesive properties of the FxFG domain Nsp1 in comparison with the hydrogel-forming property of Nsp1 (Frey et al., 2006; Frey and Gorlich, 2007, 2009). More generally, the class of GLFG domains that was postulated to favor hydrogel formation is particularly lacking in vertebrate NPCs and is only found in yeast (Table 2).

Yet, it has been suggested that the FG-domains are in a perpetual state of collapse after equating the observation of FG-domain collapse (Lim et al., 2007a) to the measured physiological Kap concentration in the NPC (Paradise et al.,

Table 2 Estimated number of FG-domains in the NPCs of *S. cerevisiae* and *H. sapiens*.

	Copies per NPC[a]	Copies per NPC[b]	Copies per NPC[c]	Copies per NPC[d]
S. cerevisiae				
Nup42	8	8	8	–
Nup49	[e]	16	16	–
Nup57	[e]	16	16	–
Nup100	[e]	32	8	–
Nup145	[e]	32	16	–
Nup116	[e]	32	8	–
Nsp1	≥32	32	32	–
Nup60	8	–	8	–
Nup159	8	8	8	–
Nup1	8	8	8	–
Nup2	[e]	–	8	–
Nup53	[e]	32	–	–
Nup59	[e]	32	–	–
H. sapiens				
Nup54	–	32	32–48	32–48
Nup62	–	16	16	16
Nup45	–	32	48	32
Nup214	–	8	8	8
Nup58	–	48	48	48
Nup98	–	8	8	8
Cg1/Nlp1	–	16	16	–
Pom121	–	8	8	8
Nup153	–	8	8	8
Nup50	–	32	32	32
Nup358	–	8	8	8

[a]Taken from Rout et al. (2000).
[b]Taken from Cronshaw et al. (2002).
[c]Taken from Terry and Wente (2009).
[d]Taken from Peters (2009b).
[e]Most of the Nups in this group are present in two copies per spoke as defined in Rout et al. (2000).

2007). According to the 'reduction of dimensionality' (ROD) model (Peters, 2005, 2009a,b), the collapsed FG-domains could effectively coat the walls of the central channel with a coherent hydrophobic 'FG-rich layer' that would promote the surface diffusion of Kap-cargo complexes. Although direct experimental evidence is still lacking, the collapsed height of approximately 10 nm for Nup153 (Lim et al., 2007a) implies that an unoccluded space at the central channel would allow small molecules to permeate through (Peters, 2005, 2009a,b).

Defining the contextual details of the NPC

A large part of the ambiguity regarding FG-domain behavior and how NPC function is regulated stems from difficulties in visualizing the FG-domains within individual NPCs. Despite obtaining high-resolution structural information of the overall NPC and its sub-complexes by cryo-electron tomography (cryo-ET; Stoffler et al., 2003; Beck et al., 2004, 2007; Elad et al., 2009; Frenkiel-Krispin et al., 2010) and

X-ray crystallography (Boehmer et al., 2008; Brohawn and Schwartz, 2009; Leksa et al., 2009; Whittle and Schwartz, 2009) respectively, several structural aspects of FG-domain behavior in the NPC remain unknown. Where are the anchoring sites of each FG-domain per Nup type? How far can the FG-domains reach into the central channel? What is the diameter of the central channel without the FG-domains? In this next section, we have constructed basic models to explore the boundary conditions and contextual details pertaining to the NPC that might influence FG-domain behavior.

FG-domains in the NPC

In Figure 2, we use drawn-to-scale illustrations to demonstrate how the contextual details of the NPC can affect the way the FG-domains look and behave inside the NPC. First of all, we have defined the NPC to take on a smooth 'hourglass-like' hyperbolic topology. Although this oversimplifies the topographical corrugations in the central channel, we aim to use the 'easiest case' to demonstrate how small differences in nanoscale features – many of which remain uncertain – can affect FG-domain behavior in the NPC. In the absence of the FG-domains, the central channel has a height (Z) of approximately 37 nm, with its narrowest (i.e., central plane) and widest diameter (i.e., both peripheries) being approximately 38 nm and approximately 98 nm, respectively, as predicted for the yeast NPC (Alber et al., 2007a,b). The volume and surface area of such a central channel is estimated to be approximately 85 000 nm^3 and approximately 15 000 nm^2, respectively. The unperturbed molecular size of each FG-domain can be defined by its hydrated hydrodynamic radius (*R*). This is a sensible approximation given that polymeric chains maintain their hydrodynamic size when end-tethered on a surface so long as the distance (*d*) between anchoring sites is more than twice the hydrodynamic radius ($d>2R$) of the polymer (i.e., forming 'mushrooms'; Degennes, 1987). Denning and colleagues have reported that the hydrodynamic radius (i.e., Stokes' radius) of *Saccharomyces cerevisiae* FG-domains lies between 4 and 8 nm depending on the specific Nup (Denning et al., 2003). Accordingly, we have calculated from these values an average unperturbed hydrodynamic radius of $R=6$ nm. For consistency, the FG-domains in Figure 2 have been drawn to scale with a line thickness reflecting the size of a single amino acid (approx. 0.4 nm).

First, we would like to address a situation where the distance between each FG-domain anchoring site is more than twice the hydrodynamic radius ($d>2R$). As defined in the cutaway view in Figure 2A, our model consists of eight planes (or levels) in the Z-axis with each level consisting of eight FG-domain anchoring sites evenly spaced around the circumference of each level (for a total of 64 FG-domains). This gives $d_Z=12.5$ nm and $d_r=15.3$ nm for the distance between anchoring sites in (i) the curved surface running along the Z-axis, and (ii) around the circumference at the central plane, respectively. In spatial terms, each hydrated FG-domain is able to maintain its hydrodynamic size (forming 'mushrooms') when tethered to each respective anchor-
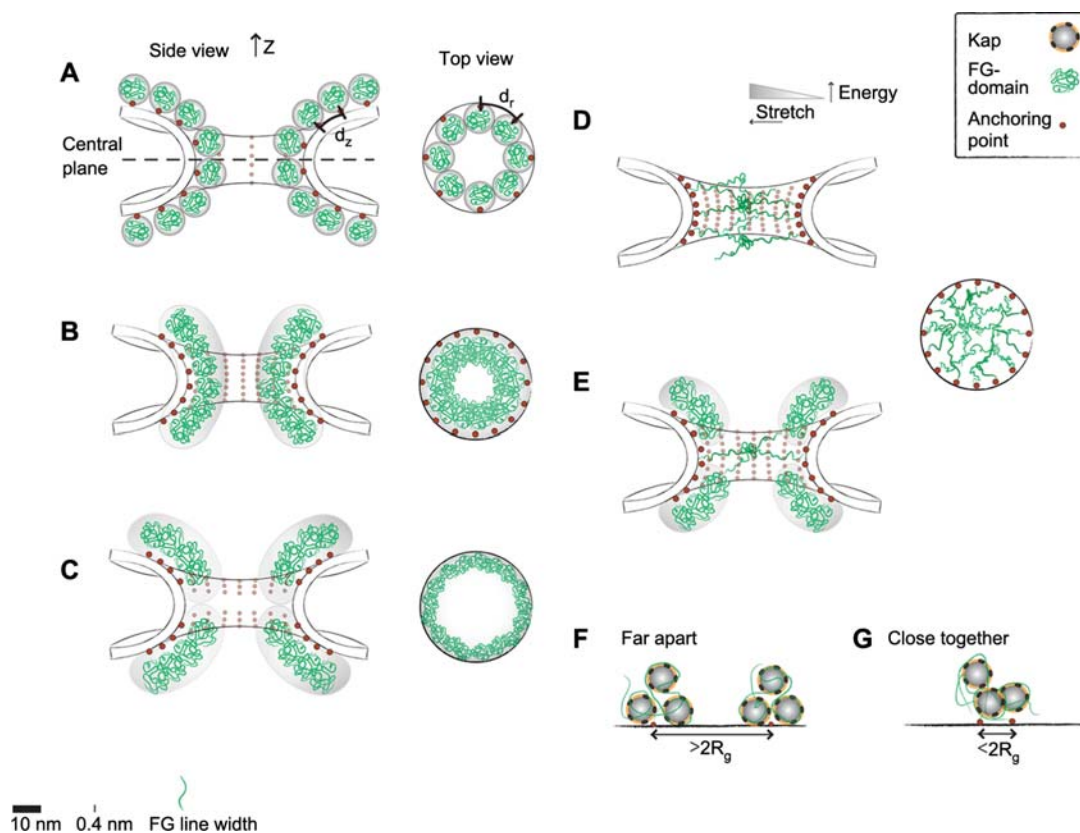
Figure 2 Defining FG-domain arrangements in the NPC.
Cutaway and top-down views of the central axis and the central plane emphasize the distribution of end-tethered FG-domains (green) and their corresponding anchoring sites (red). The drawn-to-scale dimensions of the central channel as defined by the yeast NPC (Alber et al., 2007a) with a height (Z) of ≈ 37 nm, as well as the narrowest (i.e., central plane) and widest diameters (i.e., both peripheries) being ≈ 38 nm and ≈ 98 nm, respectively. d_Z and d_r correspond to the distances between anchoring sites in the Z-axis and the circumference of the central plane, respectively. Each FG-domain is also drawn to scale with a thickness of approximately 0.4 nm. Based on the number of FG-domains and distance between anchoring sites, the FG-domains can give rise to (A) mushroom-like conformations of $R = 6$ nm where the chains do not interact with each other, (B) to a brush conformation where close packing and overlap causes the FG-domains to stretch away from the walls. (C) The uncertainty in their anchoring sites allows us to conjure a situation where the brushes are localized towards the peripheries of the central channel, leaving the inner part of the channel 'FG-domain free'. (D) Meshwork formation occurs when highly extended FG-domains are able to form strong linkages with each other across the central channel via hydrophobic inter-FG interactions or attractive electrostatic interactions. Note that a large amount of energy is required to stretch a single FG-domain across the central channel. (E) A two-gate model is illustrated where the central and peripheral FG-domains form a meshwork and brush respectively. Panels (F) and (G) illustrate plausible differences in multivalent Kap-binding between isolated FG-domains anchored far apart from each other and FG-domains anchored close together. See text for details. Note that the gray shaded areas emphasize the dynamic mobility of the FG-domains and help to demarcate the NPC repulsive barrier.

ing site leaving the central channel 'open'. Over these spatial distances, the FG-domains are unlikely to touch each other and are much less likely to occur naturally extended across the central channel. With the persistence length of a single FG-domain being on the order of a single amino acid (Lim et al., 2006), it would take a large amount of energy (i.e., approx. 10–100 k_BT) to stretch a single FG-domain from its relaxed state (defined by the hydrodynamic radius) over a distance comparable to its contour length (i.e., its maximum possible extension length; Janshoff et al., 2000) that is capable of reaching across the pore (Lim et al., 2007b). This difficulty becomes more pronounced moving outwards from the central plane towards the peripheries of the pore given

its curved hourglass-like cross-section (i.e., the FG-domains would have to be stretched over larger distances). Hence, suggestions that the FG-domains can reach across the pore some multiple times seem rather improbable considering their inherent structural flexibility and entropic elasticity.

A second scenario is shown in Figure 2B where the anchoring sites are more closely spaced. Here, the eight Z-axis planes are now defined at a distance $d_Z = 4.6$ nm. Moreover, each level now consists of 16 FG-domain anchoring sites (two multiples of eight) evenly spaced around the circumference of each level (for a total of 128 FG-domains). This gives a d_r value of 6.4 nm. In this situation, both d_r and d_Z are less than $2R$ (= 12 nm). If FG-domains were accord-

ingly tethered, their overlapping exclusion volumes would cause the FG-domains to stretch away from the surface of the central channel to maximize conformational entropy and assume the most energetically favorable state. By definition, the extended FG-domains are now in a polymer brush conformation (Degennes, 1987). A characteristic property of a polymer brush is that it gives rise to a long-range exponentially decaying steric repulsive force (Degennes, 1987) (gray shaded area in Figure 2B). This resistance to compression explains why polymer brushes are commonly used as barriers against macromolecules while remaining porous to solvent molecules (Zhou and Huck, 2006). As compared with Figure 2A, the diameter of the central channel is now greatly reduced. This forms the basic premise of the NPC brush model where the repulsive FG-domain barrier acts to 'push away' non-specific macromolecules and not just impede their passage into the NPC. A key point to note is that although brush-like behavior does not preclude any electrostatic or hydrophobic inter-FG interactions between FG-domains (Miao and Schulten, 2009), it is an important pre-requisite for FG-domain extension and stretching.

A situation where anchoring sites are lacking at the central plane is given in Figure 2C. Indeed, this is a reasonable scenario considering that the uncertainty of FG-Nup localization studies was reported as ±8 nm and ±4.5 nm along the radial and Z-axis in the yeast NPC, respectively (Alber et al., 2007b). Note that the FG-domain barrier is now predominantly located at the peripheries of the central channel. Once past the FG-domain 'corona' or 'cloud', a Kap-cargo complex could exhibit unhindered Brownian motion within the very middle of the central channel (Yang et al., 2004; Herrmann et al., 2009).

A scenario where the distance between anchoring sites is small enough can provide the driving force for the brush-like FG-domains on opposing sides to extend to the point where they would be within range to interact with each other across the central channel (Figure 2D). A survey of all FG-domains from both *S. cerevisiae* and *Homo sapiens* reveals that they contain an average of approximately 25% hydrophobic residues and up to 20% charged residues (Table 1) with more than 50% of residues in a single FG-domain being made up of disorder-conferring amino acids (Denning et al., 2003) (A,R,Q,E,G,K,P,S). Meshwork formation in the NPC will then require that the molecular linkages consisting of either hydrophobic inter-FG interactions, attractive electrostatic interactions, or both would have to be strong enough to stabilize each FG-domain. Here, it is important to bear in mind that these 'cohesion'-promoting interactions would occur in the presence of other 'non-cohesive' interactions such as electrostatic repulsion between FG-domains, steric hindrance and spatial confinement effects within the NPC. In the ensuing competition between the different interactions, the central channel would be occluded by the FG-domain meshwork if the degrees of attractive 'cohesive' interactions dominate locally over the repulsive ones. A consideration of these contextual details might explain why the equivalence of this scenario and that of macroscopic gels constructed from non-tethered FG-domains in solution (Frey et al., 2006; Frey and Gorlich, 2007, 2009) is not obvious.

Alternatively, in Figure 2E the formation of a central mesh-like sieve (i.e., comprising cohesive GLFG-domains) and peripheral brush-barriers (i.e., comprising non-cohesive FxFG-domains; similar to Figure 2B,C) could give rise to a two-gate system (Patel et al., 2007).

Finally, in Figure 2F, we show with a simple illustration how differences in the distance between anchoring sites can also influence Kap-FG domain binding. This arises owing to the fact that both Kaps and FG-domains exhibit multiple FG-binding pockets and Kap-binding FG-repeat motifs, respectively. For instance, Kapβ1 is estimated to have ten FG-binding pockets (Bayliss et al., 2000; Isgro and Schulten, 2005). Strictly hypothetically, let us assume that two similar but widely spaced FG-domains can maximally bind three Kaps each (with a characteristic binding affinity). Now, if the spacing between FG-domain anchoring sites is reduced (Figure 2G), one would find that Kap-FG binding might be more complex because the same Kaps are likely to interact with FG-repeats localized on different FG-domains. Hence, in spite of their apparent weak binding affinity, we predict that Kap-FG domain binding kinetics ought to vary as a function of FG-domain surface density (i.e., exhibiting the effect of avidity) as given by the distance between anchoring sites. If proven correct, *in vitro* binding affinity measurements would be particularly sensitive to experimental protocol and design.

Outlook

Undoubtedly these examples represent an oversimplification of the NPC. In actuality it is estimated that each NPC consists of about 200 FG-domains divided among approximately 12 different FG-Nups in both yeast (Rout et al., 2000) and vertebrate (Cronshaw et al., 2002) NPCs. Being at the nanometer molecular length scale, a primary 'boundary' condition necessitates that FG-domain behavior in the NPC will be governed by the fact that each chain is anchored to the central channel. Hence, a discrepancy remains as to whether FG-domains free-floating in bulk solution can be rationalized to behave in a comparable manner to those within the NPC. This is because parameters such as the exact position of each anchoring site and the distance between anchoring sites define the most basic structural/physical determinants that would influence FG-domain behavior and Kap-FG interactions in the NPC.

One can conduct yet another exercise to demonstrate the importance of FG-domain distribution in the (yeast) NPC. Instead of superimposing individual FG-domains into the NPC, we have labeled each FG-Nup position (estimated by Alber et al., 2007b) with an integer representing the expected number of FG-domains present per FG-Nup (taken from Terry and Wente, 2009; see Table 2). As shown in Figure 3, the most abundant FG-domains belong to the symmetric FG-Nups located close to the central plane (note: the data for Nup53 and Nup59 are not clear and have been left out). Yet, with the exception of Nsp1, Nup49 and Nup57 are compar-
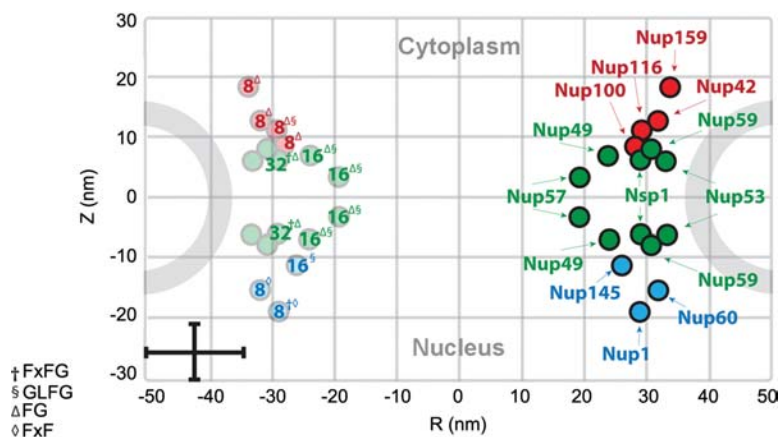
Figure 3 Estimated number of copies and positions of FG-Nups in the yeast NPC.
The symmetric FG-Nups are colored in green and the cytoplasmic and nucleoplasmic FG-Nups are colored red and blue, respectively. The number of FG-Nup copies per NPC is tabulated in Table 2 and was taken from Terry and Wente (2009). Note the error bars in the lower left-hand corner of the Figure. The superscript corresponds to the dominant FG motif of each FG-Nup. Modified with permission from Alber et al. (2007b).

atively short having a reported hydrodynamic radius of 4.1 nm and 4.7 nm, respectively (Denning et al., 2003) (see also Table 1). Being close to the central plane with an estimated number of 16 FG-domains, the distribution of Nup57 (FG/GLFG) initially shows the closest resemblance to the scenario presented in Figure 2B. As follows, we find that d_r (≈ 6.4 nm) $< 2R_{Nup57}$ ($= 9.4$ nm) and indicates that Nup57 would be in the brush-regime. If we further factor in the uncertainty regarding the anchoring sites of Nup57 (Alber et al., 2007b) (indicated by the vertical error bar in Figure 3), it is also reasonable for the NPC to be lacking FG-domains close to the central plane closely resembling the scenario presented in Figure 2C. Or, if the error in the radial distribution of Nup57 is also accounted for, it might well be that individual Nup57 FG-domains can stretch over a distance of approximately 20 nm to form a meshwork across the central channel. Upon closer inspection, it would appear that Nsp1 has the highest likelihood of forming a meshwork having a large hydrodynamic radius and being closely spaced with 32 copies. However, conflicting experimental evidence showing that yeast Nsp1 exhibits both cohesive (Frey et al., 2006; Frey and Gorlich, 2007, 2009) and non-cohesive properties (Patel et al., 2007) makes it even more difficult to predict if it forms a meshwork in the NPC.

This also raises questions related to semantics, where the FG-domains are often described as being 'filaments', 'filamentous' or even 'spaghetti-like'. Such descriptions can be potentially misleading because they imply that the FG-domains (each consisting of a single strand of amino acids) could be easily extended or structurally rigid (e.g., in a manner similar to intermediate filaments; Herrmann et al., 2007) enough to reach across the central channel on their own. If some form of macroscopic reasoning were required, the entropic elasticity of each FG-domain would be better described to resemble a single-stranded rubber band, where

it becomes (exponentially) more difficult to pull the more it is stretched.

So how can NPC topology further affect FG-domain behavior? If we assume that an hourglass correctly approximates the NPC cross-sectional curvature, the FG-domains might be increasingly oriented in an outward direction from the central pore moving away from the central plane (as depicted in Figure 2). Although the asymmetric FG-domains at the peripheries are long (with the exception of Nup145, Nup60, and Nup42), the fact that they only comprise eight FG-domains in addition to the larger diameter/circumference of the central channel at the peripheries indicates that their anchoring sites are probably more widely spaced. Similarly, spatial confinement close to the central plane might cause the FG-domains anchored there to preferentially 'reach out' of the central channel to maximize their conformational entropy (as opposed to simply coalescing in the central channel), such as has been observed for synthetic polymers (Lim and Deng, 2009).

Clearly, the NPC does not only consist of FG-domains, but also Kaps and cargoes, which interact with each other as well as the FG-domains dynamically over time. On their own, the FG-domains contribute approximately 75 000 amino acids (or alternatively approx. 3500 FG repeats). Assuming each amino acid has a volume of approximately 0.1 nm^3 (Nolting, 2006), less than 10% of the central channel by volume would be occupied by the FG-domains inside the NPC. Such a vacant depiction of the NPC can be considered to represent the 'ground state' whereby the FG-domains are not bound to any endogenous receptors and cargoes. If such a state could be achieved *in situ*, this could allow for subsequent changes in the FG-domains to be investigated and rationalized with model predictions. For instance, can Figure 2B and Figure 2A reasonably depict the central channel before and after 50% of the FG-domains have been deleted

(Strawn et al., 2004)? In the case of cargo import, FG-domain behavior might be tested for any changes occurring before and after Kap binding. Could the conformational changes observed for Nup153 before and after binding Kapβ1 be more general to other FG-domains? Likewise, the premise of the selective phase model predicts that Kaps compete with the hydrophobic inter-FG interactions to transiently 'open' the meshwork so as to provide more space for diffusion to proceed (Ribbeck and Gorlich, 2001; Frey et al., 2006; Frey and Gorlich, 2007, 2009). Could one test for a physical swelling of the FG-domain meshwork in the NPC that de-swells back to its crosslinked state once import is completed? Can both the brush and meshwork FG-domain conformations help in minimizing non-specific clogging at the NPC?

Looking ahead, the following questions could perhaps allow us to glean further insight as to how the FG-domains contribute to NPC functionality: how far apart are the FG-domain anchoring sites (i) in the direction parallel to the NPC Z-axis, and (ii) along the circumference of the NPC? Can the FG-domains interact with the structured walls of the central channel? How strong are inter-FG interactions under stretched FG-domain conditions? How do repulsive interactions (e.g., electrostatic, steric) compete against attractive interactions (e.g., inter-FG hydrophobic, electrostatic) between the FG-domains? Can their resulting degrees of interaction be quantified in the NPC? What is the degree of hydrophobicity required to define a specific Kap-FG interaction (in light of recent evidence showing that a degree of hydrophobic character is needed for non-specific translocation to proceed; Naim et al., 2009)? Is the observed Brownian motion of Kap-cargo complexes within the NPC (Herrmann et al., 2009) dependent on FG-domain behavior? How does a Kap slide and can Kap-sliding be promoted along a collapsed FG-domain surface? On a related note, the dynamic time-scales of Kap-FG interactions remain wholly unknown. What are the relevant timescales that describe single molecule Kap-FG interactions? What are the relaxation times of the FG-domains after Kap release? Does a continuous presence of Kaps in the central channel imply that the FG-domains are always collapsed? Last but not least, do the FG-domains in different species display the same functional characteristics based on differences in NPC size and structure (Figure 1)?

Understanding FG-domain behavior has presented major challenges given that natively unfolded/intrinsically disordered systems are less well understood in biology. In this review, we have introduced basic concepts in polymer physics that illustrate a collective convergence towards rationalizing unfolded FG-domain function in the NPC. These can be particularly useful in making direct experimental and theoretical correlations, and sets the next stage of investigation where interdisciplinary efforts will be required to obtain a rigorous understanding of FG-domain behavior at the relevant length scales, topologies and timescales. Clearly, our understanding of NPC functionality will be further bolstered by a deeper appreciation for the contextual details governing FG-domain behavior with relevance to other intrinsically dis-

ordered biological molecules and systems (Tompa et al., 2009).

Concluding remarks

During the final stages of preparing for this review, we came across four newly published papers that deserve worthy mention. Of special interest is a study by Ma and Yang, who mapped in three dimensions the spatial density of interaction sites between importinβ1 and the FG-domains in the NPC using single-point edge-excitation subdiffraction (SPEED) microscopy (Figure 4) (Ma and Yang, 2010). In addition to finding that their interactions increased from the NPC peripheries towards the central pore, the authors reported that there exists a 10–20-nm-diameter tube-like region at the center of the NPC that is rarely occupied by both cargo-free and cargo-bound importinβ1 (i.e., suggesting a lack of FG-domains there). This indicates that the FG-interaction zone in the NPC spans a radial distance of approximately 20 nm from the inner wall of the central channel towards the central axis. Being larger than the hydrodynamic size of a FG-domain might indicate a brush-like extension of the FG-domains (compare with Figure 2B). Their data also highlighted distinctively the NPC barrier-region where receptor-free cargoes were occluded in the absence of importinβ1. Clearly, the overlap between the receptor-FG interaction zone and the barrier region underscores the dualistic role of the FG-domains to promote and hinder cargo translocation. At least in part, the cytoplasmic approach pathway of receptor-free cargoes that is gradually hindered at the central plane suggests that a conformational change in the FG-domains [e.g., brush re-extension (Lim et al., 2007a) and/or meshwork re-sealing (Frey and Gorlich, 2009); compare with Figure 2E] might have occurred in the absence of importinβ1. As suggested by the ROD model (Peters, 2005, 2009a,b), this implies that the FG-domains are less extended (i.e., or partially collapsed) under physiological transport conditions.

Next, two separate papers (Ader et al., 2010; Yamada et al., 2010) now show corroborating evidence that could help to dispel the conflicting experimental evidence that yeast Nsp1 is both cohesive (Frey et al., 2006; Frey and Gorlich, 2007, 2009) and non-cohesive (Patel et al., 2007). Here, both groups report that the FG-domain of Nsp1 contains both a cohesive and non-cohesive region in its N- and C-terminal parts, respectively. Moreover, Yamada et al. demonstrate that regions of FG-domains can be globularly compact (cohesive) and extended (repulsive) depending on their low charge and high charge content, respectively. This is in agreement with predictions (Bright et al., 2001) that intrinsically unstructured proteins can exhibit polyampholytic behavior (i.e., charged polymers consisting of both positively and negatively charged groups).

Finally, Eisele et al. used two-dimensional planar lipid bilayers to produce densely tethered FG-domains (Nsp1) that were extended to approximately 35 nm in length (Eisele et al., 2010). They showed that Kap95 (importinβ from *S. cerevisiae*) could efficiently enter, permeate and leave the FG-
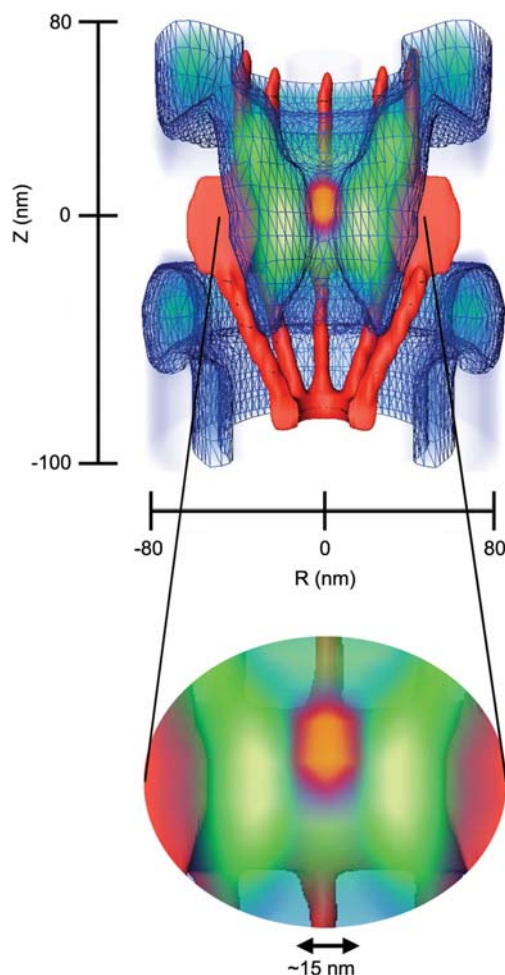
Figure 4 Three-dimensional spatial density of receptor-cargo and FG-domain interaction sites in the NPC (blue: lower density, green: higher density) as revealed by single-point edge-excitation subdiffraction (SPEED) microscopy (Ma and Yang, 2010).

Note that the high-density areas (green) suggest that the FG-domains are extended at a length of approximately 20 nm from the surface of the central channel (red) towards the central axis (compare with Figure 2B). A 15-nm-diameter axial region at the center of the NPC is rarely occupied by both cargo-free and cargo-bound importinβ1 (i.e., suggesting a lack of FG-domains there). In the absence of importinβ1, the green area also demarcates the range of the FG-domain barrier in the NPC where the passage of receptor-free cargoes on approach from the cytoplasm is hindered close to the central plane (orange zone). Modified from Ma and Yang (2010).

might not be mutually exclusive in the NPC. From here on, it remains instructive to account for the key contextual details in trying to understand how the various FG-domain effects and their differing degrees of interaction contribute to the selective transport of cargoes through the NPC.

domains without affecting the global morphology of the FG-domain film (i.e., no collapse was observed). Although the authors interpreted this finding in the context of meshwork formation within the film, the fact that the FG-domains were extended about 35 nm away from the bilayer surface indicates (by definition) a brush-like characteristic in the FG-domains.

In conclusion, our survey of the current evidence on FG-domain behavior converges on the point that extended brush-like behavior and the formation of meshwork-like linkages

References

Ader, C., Frey, S., Maas, W., Schmidt, H.B., Gorlich, D., and Baldus, M. (2010). Amyloid-like interactions within nucleoporin FG hydrogels. Proc. Natl. Acad. Sci. USA, Epub ahead of print, DOI: 10.1073/pnas.0910163107.

Alber, F., Dokudovskaya, S., Veenhoff, L.M., Zhang, W.H., Kipper, J., Devos, D., Suprapto, A., Karni-Schmidt, O., Williams, R., Chait, B.T., et al. (2007a). The molecular architecture of the nuclear pore complex. Nature *450*, 695–701.

Alber, F., Dokudovskaya, S., Veenhoff, L.M., Zhang, W.Z., Kipper, J., Devos, D., Suprapto, A., Karni-Schmidt, O., Williams, R., Chait, B.T., et al. (2007b). Determining the architectures of macromolecular assemblies. Nature *450*, 683–694.

Bayliss, R., Ribbeck, K., Akin, D., Kent, H.M., Feldherr, C.M., Gorlich, D., and Stewart, M. (1999). Interaction between NTF2 and xFxFG-containing nucleoporins is required to mediate nuclear import of RanGDP. J. Mol. Biol. *293*, 579–593.

Bayliss, R., Littlewood, T., and Stewart, M. (2000). Structural basis for the interaction between FxFG nucleoporin repeats and importin-β in nuclear trafficking. Cell *102*, 99–108.

Bayliss, R., Leung, S.W., Baker, R.P., Quimby, B.B., Corbett, A.H., and Stewart, M. (2002a). Structural basis for the interaction between NTF2 and nucleoporin FxFG repeats. EMBO J. *21*, 2843–2853.

Bayliss, R., Littlewood, T., Strawn, L.A., Wente, S.R., and Stewart, M. (2002b). GLFG and FxFG nucleoporins bind to overlapping sites on importin-β. J. Biol. Chem. *277*, 50597–50606.

Beck, M., Forster, F., Ecke, M., Plitzko, J.M., Melchior, F., Gerisch, G., Baumeister, W., and Medalia, O. (2004). Nuclear pore complex structure and dynamics revealed by cryoelectron tomography. Science *306*, 1387–1390.

Beck, M., Lucic, V., Forster, F., Baumeister, W., and Medalia, O. (2007). Snapshots of nuclear pore complexes in action captured by cryo-electron tomography. Nature *449*, 611–615.

Bednenko, J., Cingolani, G., and Gerace, L. (2003). Importin β contains a COOH-terminal nucleoporin binding region important for nuclear transport. J. Cell Biol. *162*, 391–401.

Belfort, G., Davis, R.H., and Zydney, A.L. (1994). The behavior of suspensions and macromolecular solutions in cross-flow microfiltration. J. Membr. Sci. *96*, 1–58.

Ben-Efraim, I. and Gerace, L. (2001). Gradient of increasing affinity of importin β for nucleoporins along the pathway of nuclear import. J. Cell Biol. *152*, 411–417.

Boehmer, T., Jeudy, S., Berke, I.C., and Schwartz, T.U. (2008). Structural and functional studies of Nup107/Nup133 interaction and its implications for the architecture of the nuclear pore complex. Mol. Cell *30*, 721–731.

Bright, J.N., Woolf, T.B., and Hoh, J.H. (2001). Predicting properties of intrinsically unstructured proteins. Prog. Biophys. Mol. Biol. *76*, 131–173.

Brohawn, S.G. and Schwartz, T.U. (2009). Molecular architecture of the Nup84-Nup145C-Sec13 edge element in the nuclear pore complex lattice. Nat. Struct. Mol. Biol. *16*, 1173–U1178.

Conti, E., Muller, C.W., and Stewart, M. (2006). Karyopherin flexibility in nucleocytoplasmic transport. Curr. Opin. Struct. Biol. *16*, 237–244.

Cronshaw, J.A., Krutchinsky, A.N., Zhang, W.Z., Chait, B.T., and Matunis, M.J. (2002). Proteomic analysis of the mammalian nuclear pore complex. J. Cell Biol. *158*, 915–927.

Cushman, I., Palzkill, T., and Moore, M.S. (2006). Using peptide arrays to define nuclear carrier binding sites on nucleoporins. Methods *39*, 329–341.

D'angelo, M.A. and Hetzer, M.W. (2008). Structure, dynamics and function of nuclear pore complexes. Trends Cell Biol. *18*, 456–466.

Degennes, P.G. (1987). Polymers at an interface – a simplified view. Adv. Colloid Interfac. *27*, 189–209.

Denning, D.P., Patel, S.S., Uversky, V., Fink, A.L., and Rexach, M. (2003). Disorder in the nuclear pore complex: the FG repeat regions of nucleoporins are natively unfolded. Proc. Natl. Acad. Sci. USA *100*, 2450–2455.

Devos, D., Dokudovskaya, S., Williams, R., Alber, F., Eswar, N., Chait, B.T., Rout, M.P., and Sali, A. (2006). Simple fold composition and modular architecture of the nuclear pore complex. Proc. Natl. Acad. Sci. USA *103*, 2172–2177.

Eisele, N.B., Frey, S., Piehler, J., Gorlich, D., and Richter, R.P. (2010). Ultrathin nucleoporin phenylalanine-glycine repeat films and their interaction with nuclear transport receptors. EMBO Rep., Epub ahead of print, DOI:10.1038/embor.2010.34.

Elad, N., Maimon, T., Frenkiel-Krispin, D., Lim, R.Y.H., and Medalia, O. (2009). Structural analysis of the nuclear pore complex by integrated approaches. Curr. Opin. Struct. Biol. *19*, 226–232.

Fahrenkrog, B., Maco, B., Fager, A.M., Koser, J., Sauder, U., Ullman, K.S., and Aebi, U. (2002). Domain-specific antibodies reveal multiple-site topology of Nup153 within the nuclear pore complex. J. Struct. Biol. *140*, 254–267.

Frenkiel-Krispin, D., Maco, B., Aebi, U., and Medalia, O. (2010). Structural analysis of a metazoan nuclear pore complex reveals a fused concentric ring architecture. J. Mol. Biol. *395*, 578–586.

Frey, S. and Gorlich, D. (2007). A saturated FG-repeat hydrogel can reproduce the permeability properties of nuclear pore complexes. Cell *130*, 512–523.

Frey, S. and Gorlich, D. (2009). FG/FxFG as well as GLFG repeats form a selective permeability barrier with self-healing properties. EMBO J. *28*, 2554–2567.

Frey, S., Richter, R.P., and Goerlich, D. (2006). FG-rich repeats of nuclear pore proteins form a three-dimensional meshwork with hydrogel-like properties. Science *314*, 815–817.

Gorlich, D. and Kutay, U. (1999). Transport between the cell nucleus and the cytoplasm. Annu. Rev. Cell. Dev. Biol. *15*, 607–660.

Gorlich, D., Pante, N., Kutay, U., Aebi, U., and Bischoff, F.R. (1996). Identification of different roles for RanGDP and RanGTP in nuclear protein import. EMBO J. *15*, 5584–5594.

Herrmann, H., Bar, H., Kreplak, L., Strelkov, S.V., and Aebi, U. (2007). Intermediate filaments: from cell architecture to nanomechanics. Nat. Rev. Mol. Cell Biol. *8*, 562–573.

Herrmann, M., Neuberth, N., Wissler, J., Perez, J., Gradl, D., and Naber, A. (2009). Near-field optical study of protein transport kinetics at a single nuclear pore. Nano. Lett. *9*, 3330–3336.

Hong, S.K. and Elimelech, M. (1997). Chemical and physical aspects of natural organic matter (NOM) fouling of nanofiltration membranes. J. Membr. Sci. *132*, 159–181.

Isgro, T.A. and Schulten, K. (2005). Binding dynamics of isolated nucleoporin repeat regions to importin-β. Structure *13*, 1869–1879.

Janshoff, A., Neitzert, M., Oberdorfer, Y., and Fuchs, H. (2000). Force spectroscopy of molecular systems-single molecule spectroscopy of polymers and biomolecules. Angew. Chem. Int. Ed. *39*, 3213–3237.

Jovanovic-Talisman, T., Tetenbaum-Novatt, J., McKenney, A.S., Zilman, A., Peters, R., Rout, M.P., and Chait, B.T. (2009). Artificial nanopores that mimic the transport selectivity of the nuclear pore complex. Nature *457*, 1023–1027.

Keminer, O. and Peters, R. (1999). Permeability of single nuclear pores. Biophys. J. *77*, 217–228.

Koehler, J.A., Ulbricht, M., and Belfort, G. (1997). Intermolecular forces between proteins and polymer films with relevance to filtration. Langmuir *13*, 4162–4171.

Kustanovich, T. and Rabin, Y. (2004). Metastable network model of protein transport through nuclear pores. Biophys. J. *86*, 2008–2016.

Leksa, N.C., Brohawn, S.G., and Schwartz, T.U. (2009). The structure of the scaffold nucleoporin Nup120 reveals a new and unexpected domain architecture. Structure *17*, 1082–1091.

Lim, R.Y.H. and Deng, J. (2009). Interaction forces and reversible collapse of a polymer brush-gated nanopore. ACS Nano. *3*, 2911–2918.

Lim, R.Y.H., Huang, N.P., Koser, J., Deng, J., Lau, K.H.A., Schwarz-Herion, K., Fahrenkrog, B., and Aebi, U. (2006). Flexible phenylalanine-glycine nucleoporins as entropic barriers to nucleocytoplasmic transport. Proc. Natl. Acad. Sci. USA *103*, 9512–9517.

Lim, R.Y.H., Fahrenkrog, B., Koser, J., Schwarz-Herion, K., Deng, J., and Aebi, U. (2007a). Nanomechanical basis of selective gating by the nuclear pore complex. Science *318*, 640–643.

Lim, R.Y.H., Koser, J., Huang, N.P., Schwarz-Herion, K., and Aebi, U. (2007b). Nanomechanical interactions of phenylalanine-glycine nucleoporins studied by single molecule force-volume spectroscopy. J. Struct. Biol. *159*, 277–289.

Lim, R.Y.H., Aebi, U., and Fahrenkrog, B. (2008). Towards reconciling structure and function in the nuclear pore complex. Histochem. Cell Biol. *129*, 105–116.

Lusk, C.P., Blobel, G., and King, M.C. (2007). Highway to the inner nuclear membrane: rules for the road. Nat. Rev. Mol. Cell Biol. *8*, 414–420.

Ma, J. and Yang, W. (2010). Three-dimensional distribution of transient interactions in the nuclear pore complex obtained from single-molecule snapshots. Proc. Natl. Acad. Sci. USA, Epub ahead of print, DOI: 10.1073/pnas.0908269107.

Macara, I.G. (2001). Transport into and out of the nucleus. Microbiol. Mol. Biol. Rev. *65*, 570–594.

Miao, L.L. and Schulten, K. (2009). Transport-related structures and processes of the nuclear pore complex studied through molecular dynamics. Structure *17*, 449–459.

Minko, S. (2006). Responsive polymer brushes. Polym. Rev. *46*, 397–420.

Naim, B., Zbaida, D., Dagan, S., Kapon, R., and Reich, Z. (2009). Cargo surface hydrophobicity is sufficient to overcome the nuclear pore complex selectivity barrier. EMBO J. *28*, 2697–2705.

Nolting, B. (2006). Protein Folding Kinetics: Biophysical Methods, Second Edition (Berlin, Germany: Springer-Verlag).

Paradise, A., Levin, M.K., Korza, G., and Carson, J.H. (2007). Significant proportions of with reduced intracellular nuclear transport proteins mobilities resolved by fluorescence correlation spectroscopy. J. Mol. Biol. *365*, 50–65.

Patel, S.S., Belmont, B.J., Sante, J.M., and Rexach, M.F. (2007). Natively unfolded nucleoporins gate protein diffusion across the nuclear pore complex. Cell *129*, 83–96.

Pemberton, L.F. and Paschal, B.M. (2005). Mechanisms of receptor-mediated nuclear import and nuclear export. Traffic *6*, 187–198.

Peters, R. (2005). Translocation through the nuclear pore complex: selectivity and speed by reduction-of-dimensionality. Traffic *6*, 421–427.

Peters, R. (2009a). Functionalization of a nanopore: the nuclear pore complex paradigm. BBA Mol. Cell Res. *1793*, 1533–1539.

Peters, R. (2009b). Translocation through the nuclear pore: kaps pave the way. Bioessays *31*, 466–477.

Pyhtila, B. and Rexach, M. (2003). A gradient of affinity for the karyopherin Kap95p along the yeast nuclear pore complex. J. Biol. Chem. *278*, 42699–42709.

Radu, A., Blobel, G., and Moore, M.S. (1995). Identification of a protein complex that is required for nuclear-protein import and mediates docking of import substrate to distinct nucleoporins. Proc. Natl. Acad. Sci. USA *92*, 1769–1773.

Reichelt, R., Holzenburg, A., Buhle, E.L., Jarnik, M., Engel, A., and Aebi, U. (1990). Correlation between structure and mass-distribution of the nuclear-pore complex and of distinct pore complex components. J. Cell Biol. *110*, 883–894.

Rexach, M. and Blobel, G. (1995). Protein import into nuclei-association and dissociation reactions involving transport substrate, transport factors, and nucleoporins. Cell *83*, 683–692.

Ribbeck, K. and Gorlich, D. (2001). Kinetic analysis of translocation through nuclear pore complexes. EMBO J. *20*, 1320–1330.

Ribbeck, K. and Gorlich, D. (2002). The permeability barrier of nuclear pore complexes appears to operate via hydrophobic exclusion. EMBO J. *21*, 2664–2671.

Rout, M.P. and Blobel, G. (1993). Isolation of the yeast nuclear-pore complex. J. Cell Biol. *123*, 771–783.

Rout, M.P., Aitchison, J.D., Magnasco, M.O., and Chait, B.T. (2003). Virtual gating and nuclear transport: the hole picture. Trends Cell Biol. *13*, 622–628.

Rout, M.P., Aitchison, J.D., Suprapto, A., Hjertaas, K., Zhao, Y.M., and Chait, B.T. (2000). The yeast nuclear pore complex: composition, architecture, and transport mechanism. J. Cell Biol. *148*, 635–651.

Shulga, N. and Goldfarb, D.S. (2003). Binding dynamics of structural nucleoporins govern nuclear pore complex permeability and may mediate channel gating. Mol. Cell. Biol. *23*, 534–542.

Stewart, M. (2007). Molecular mechanism of the nuclear protein import cycle. Nat. Rev. Mol. Cell Biol. *8*, 195–208.

Stoffler, D., Feja, B., Fahrenkrog, B., Walz, J., Typke, D., and Aebi, U. (2003). Cryo-electron tomography provides novel insights into nuclear pore architecture: implications for nucleocytoplasmic transport. J. Mol. Biol. *328*, 119–130.

Strawn, L.A., Shen, T.X., Shulga, N., Goldfarb, D.S., and Wente, S.R. (2004). Minimal nuclear pore complexes define FG repeat domains essential for transport. Nat. Cell Biol. *6*, 197–206.

Terry, L.J. and Wente, S.R. (2009). Flexible gates: dynamic topologies and functions for FG nucleoporins in nucleocytoplasmic transport. Eukaryot. Cell *8*, 1814–1827.

Tompa, P., Fuxreiter, M., Oldfield, C.J., Simon, I., Dunker, A.K., and Uversky, V.N. (2009). Close encounters of the third kind: disordered domains and the interactions of proteins. Bioessays *31*, 328–335.

Whittle, J.R.R. and Schwartz, T.U. (2009). Architectural nucleoporins Nup157/170 and Nup133 are structurally related and descend from a second ancestral element. J. Biol. Chem. *284*, 28442–28452.

Yamada, J., Phillips, J.L., Patel, S., Goldfien, G., Calestagne-Morelli, A., Huang, H., Reza, R., Acheson, J., Krishnan, V.V., Newsam, S., et al. (2010). A bimodal distribution of two distinct categories of intrinsically disordered structures with separate functions in FG nucleoporins. Mol. Cell Proteomics, Epub ahead of print, DOI: 10.1074/mcp.M000035-MCP201.

Yang, Q., Rout, M.P., and Akey, C.W. (1998). Three-dimensional architecture of the isolated yeast nuclear pore complex: functional and evolutionary implications. Mol. Cell *1*, 223–234.

Yang, W.D., Gelles, J., and Musser, S.M. (2004). Imaging of single-molecule translocation through nuclear pore complexes. Proc. Natl. Acad. Sci. USA *101*, 12887–12892.

Zhou, F. and Huck, W.T.S. (2006). Surface grafted polymer brushes as ideal building blocks for 'smart' surfaces. Phys. Chem. Chem. Phys. *8*, 3815–3823.

Zimmerman, S.B. and Minton, A.P. (1993). Macromolecular crowding – biochemical, biophysical, and physiological consequences. Annu. Rev. Biophys. Biomol. Struct. *22*, 27–65.